Check for updates

View Article Online
View Journal

PCCP
Physical Chemistry Chemical Physics

Accepted Manuscript

This article can be cited before page numbers have been issued, to do this please use: S. Rani and S. J. Ray, *Phys. Chem. Chem. Phys.*, 2020, DOI: 10.1039/D0CP00546K.

This is an Accepted Manuscript, which has been through the Royal Society of Chemistry peer review process and has been accepted for publication.

Accepted Manuscripts are published online shortly after acceptance, before technical editing, formatting and proof reading. Using this free service, authors can make their results available to the community, in citable form, before we publish the edited article. We will replace this Accepted Manuscript with the edited and formatted Advance Article as soon as it is available.

You can find more information about Accepted Manuscripts in the Information for Authors.

Please note that technical editing may introduce minor changes to the text and/or graphics, which may alter content. The journal's standard Terms & Conditions and the Ethical guidelines still apply. In no event shall the Royal Society of Chemistry be held responsible for any errors or omissions in this Accepted Manuscript or any consequences arising from the use of any information it contains.

ROYAL SOCIETY OF CHEMISTRY

rsc.li/pccp

View Article Online
DOI: 10.1039/D0CP00546K

Two-dimensional C_3N based sub-10 nanometer Biosensor

S. Rani[1], S. J. Ray[1*]

[1] *Department of Physics, Indian Institute of Technology Patna, Bihta 801106, India*

Published on 08 April 2020. Downloaded by Université de Paris on 4/11/2020 4:02:23 PM.

Abstract

Detection and sequencing of various nucleobases are of immense usefulness that can revolutionise future medical diagnostics procedures. On the other hand, the newly discovered 2D material, C_3N has demonstrated supreme potential for future nanoelectronic and spintronic developments due to its unique sets of electronic properties and structural similarity with graphene. Here, we have investigated the effect of various nucleobases in the close vicinity of a C_3N nanoribbon. Our extensive calculations revealed significant changes in the transport behaviour in the presence of DNA/RNA molecules. The transport response can be further modified through the (i) incorporation of doping, (ii) presence of defects and (iii) concentration of the adsorbed molecule etc. Furthermore, in the the presence of a gate voltage in a Field-effect transistor (FET) geometry, the conductivity response can be improved significantly with a change $\sim 100\%$ in the presence of an adsorbed molecule. The observation of negative differential resistance (NDR) in the C_3N system has also been reported here for the first time. Our current observation demonstrates the usefulness of C_3N system as a next generation bio-sensor for the sequencing of various nucleobases, offering new leads for future developments in bioelectronics, superior sensing architectures and sustainable designs.

Physical Chemistry Chemical Physics Accepted Manuscript

*Electronic address: ray@iitp.ac.in, ray.sjr@gmail.com

View Article Online
DOI: 10.1039/D0CP00546K

Published on 08 April 2020. Downloaded by Université de Paris on 4/11/2020 4:02:23 PM.

Physical Chemistry Chemical Physics Accepted Manuscript

I. INTRODUCTION

Biosensors are of crucial importance for medical diagnostics, environmental monitoring, forensic investigation, security purposes etc. The advent of nanotechnology shows promises towards the development of various nanoscale biosensors to offer rapid detection sensitivity. The study of DNA detection and sequencing is indispensable for the cure of various types of diseases and future medical development. The Sanger method [1] has been traditionally used for sequencing of various DNA nucleobases, while in the recent times, nanopore based sequencing methods [2–6] have been at the centre of attention due to its reduced cost and simple design. Several recent developments have opened up the possibility of designing nanopores [7–9] with faster operational performance through easier fabrication routes which can be integrated for further scaling in various nanoelectronic architecture [10].

Among various 2D materials, Graphene, the first of its kind offers excellent mechanical as well as electronic properties [11–13], but the absence of band gap limits its application potential for switching and transistor design. The semiconducting state in this Dirac Fermionic [14] structure can be introduced through Nitrogen (N) doping by varying the N/C ratio, which has led to the recent discovery of 2D-polyaniline (C_3N) in mono-layered structure. In the 2D geometry, it forms a hexagonal honeycomb lattice similar to that of Graphene which was synthesised recently [15, 16]. In the recent investigations, 2D-C_3N was found to be a hole-free indirect bandgap semiconductor with fascinating electronic [17–21], mechanical [19], thermal [22, 23] and chemical [24–28] properties. In Field-effect transistor geometry, an ultra-high ON/OFF ratio $\sim 5.5 \times 10^{10}$ was observed (significantly higher than any standalone 2D-layer system) with carrier mobilities $\sim 180(220)$ $cm^2V^{-1}s^{-1}$ [16].

Due to the enhanced surface to volume ratio, 2D materials have been found to be sensitive to the presence of a neighbouring molecule [29–34]. In the current work, First-principles based calculations are used to investigate the effect of the presence of various DNA/RNA molecules on the transport properties of a Zigzag C_3N nanoribbon (ZNR). Using Non-equilibrium Green's Function (NEGF) formalism, the current-voltage characteristics of the ZNR was studied in 2-probe geometry in the presence and absence of the nucleobases. Furthermore, we investigated the effect of (boron/sulphur) doping and defects at various (edge/middle) locations on the ZNR. In addition, in a Field-effect transistor (FET) structure, a gate voltage was used to fine-tune the transport properties. The changes in transport

View Article Online
DOI: 10.1039/D0CP00546K

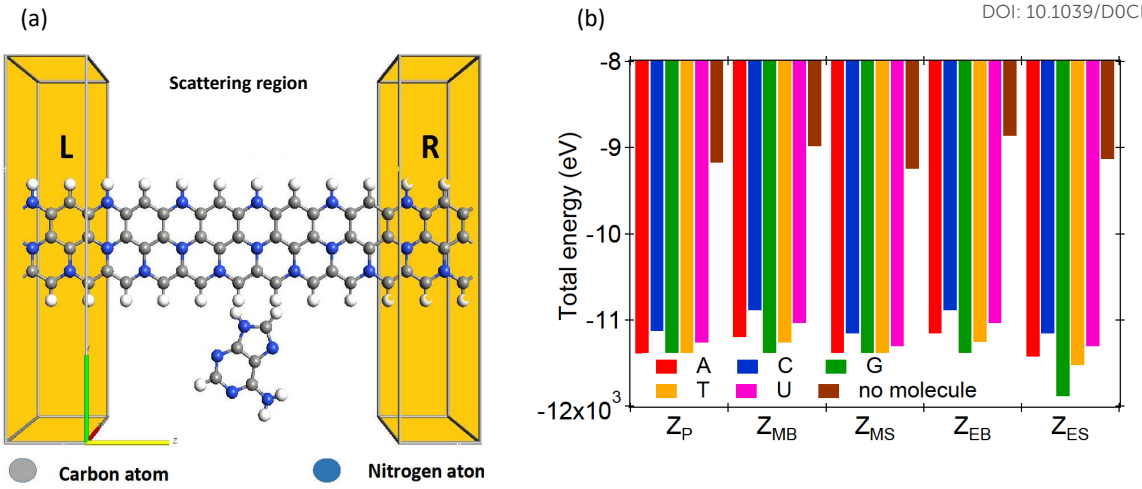

FIG. 1: (a) Schematic representation of a C_3N nanoribbon in a two probe configuration, consisting of three parts, left electrode, right electrode and central scattering region. (b) The total energy of C_3N nanoribbon in various adsorbed/doped configurations.

properties after attaching DNA/RNA molecules indicates that it can be used in future biosensing applications and sequencing of nucleobases.

II. COMPUTATIONAL METHOD

First-principles based calculations were performed to explore the electronic and transport properties of the C_3N nanoribbon. The transport properties in a two-probe configuration were calculated using a Non-equilibrium Green's Function (NEGF) [35] methodology combined with Density Functional Theory (DFT) using Atomistic Toolkit [36]. The self-consistent calculations were performed under the Gradient Generalised Approximation (GGA) of the Perdew-Burke-Ernzerhof [37] exchange-correlational functional using double-ζ polarised basis set and an energy cut-off limit of 185 Hartree. To avoid the interaction between actual simulation box and its repeat image, a minimum vacuum space of 15 Å was used along the non-periodic directions. Structural optimisation was performed before starting any calculation by ensuring the force on each atom to be lesser than 10^{-3} eV/Å.

For the transport calculations, periodic boundary condition was set along the transport direction with a Monkhorst-Pack [38] k-grid of $1 \times 1 \times 300$ (300 along the transport direction) ensuring a convergence in the transmission behaviour. Within the NEGF formalism,

Published on 08 April 2020. Downloaded by Université de Paris on 4/11/2020 4:02:23 PM.

Physical Chemistry Chemical Physics Accepted Manuscript

View Article Online
DOI: 10.1039/D0CP00546K

TABLE I: Nomenclature of the C_3N nanoribbon in various cases

Name	Description
Z_P	Pristine C_3N nanoribbon
Z_{MB}	Middle atom of C_3N doped with boron
Z_{MS}	Middle atom of C_3N doped with sulphur
Z_{EB}	Edge atom of C_3N doped with boron
Z_{ES}	Edge atom of C_3N doped with sulphur
Z_{PA}	Adenine molecule attached on the edge of pristine C_3N
Z_{PC}	Cytosine molecule attached on the edge of pristine C_3N
Z_{PG}	Guanine molecule attached on the edge of C_3N
Z_{PT}	Thymine molecule attached on the edge of C_3N
Z_{PU}	Uracil molecule attached on the edge of C_3N.

the current was estimated using the Landauer-B*ü*ttiker formula [39, 40] given by,

$$I = \frac{2e}{\hbar}\int_{-eV/2}^{eV/2} T(E,V)[f_L(E-\mu_L) - f_R(E-\mu_R)]dE \quad (1)$$

where T(E,V) is the transmission function at an energy E, bias voltage V and $f_{L/R}(E,\mu_{L/R})$ is the Fermi distribution and μ_{L} and μ_{R} are the electrochemical potentials of the left and right electrodes respectively.

III. SYSTEM DESCRIPTION

The central structure used in this investigation is a 11 × 2 supercell of zigzag C_3N nanoribbon. The C-C and C-N bond lengths of C_3N are 1.404 Å and 1.403 Å respectively. The unit cell of C_3N has a lattice constant of $\mathbf{a}$ = 4.862 Å , $\mathbf{b}$ = 4.862 Å along the zigzag and armchair directions respectively [10, 21]. We have used various acronyms to represent different configuration considered in this work, which are named as the following; (i) Z for Zigzag, (ii) P for pristine, (iii) M and E represent middle and edge locations and (iv) B, S symbolise boron and sulphur doped atoms. A total of five DNA/RNA molecules were used in this investigation, which are Adenine (A), Cytosine (C), Guanine (G), Thymine (T) and Uracil (U). A list containing the details of such nomenclature is given in Table 1 and the rest can be found be Table S1 in the supporting information [41].

Published on 08 April 2020. Downloaded by Université de Paris on 4/11/2020 4:02:23 PM.

Physical Chemistry Chemical Physics Accepted Manuscript

View Article Online
DOI: 10.1039/D0CP00546K

Published on 08 April 2020. Downloaded by Université de Paris on 4/11/2020 4:02:23 PM.

Physical Chemistry Chemical Physics Accepted Manuscript

IV. RESULTS AND DISCUSSIONS

A. Pristine system

A sample schematic explaining the 2-probe transport geometry of the ZNR is shown in Fig. 1a. Two semi-infinite electrodes are connected to the central scattering region from left and right sides, named as L/R electrodes. In the 2-probe geometry, it was observed that the planar adsorption configuration (ZNR and Molecule in the same plane) considered here offers maximum energy advantages for all the molecules and therefore, this configuration is used throughout this work as also illustrated for different molecules in Fig.S1 in the Supporting Information (SI) [41]. The total energy of Z_P was found to be -9171.9 eV, whereas in the adsorbed configuration, it reduces significantly (< -11124 eV) for Z_{PA}, Z_{PC}, Z_{PG}, Z_{PT} and Z_{PU} as shown in Fig. 1b. Such reduction in energy is possible as a result of the interaction between the energy levels of C_3N and attached molecules. As we compare results between them, the maximum reduction in energy was estimated to be 28.89% for Z_{PG}. In the adsorbed configuration, the carriers can delocalise over a larger space on the nanoribbbon, resulting in a further lowering of the energy and it also holds true for other molecules in their adsorbed configurations. Details of the adsorption energy of the nucleobases has been shown in Fig. SI9 of the SI [41].

The current-voltage (I-V) characteristics of the ZNR in the pristine and adsorbed (with Adenine) configuration has been illustrated in Fig.2a. In the pristine configuration, an increase in current can be observed from V = 0 towards the higher voltages. However, in the adsorbed configuration, a reduction in current is found at higher voltages as a result of the additional scattering induced by the attached molecules on the ZNR. It is also visible from the transmission spectrum in these two cases as shown in Fig.2b. The maximum conduction states lies around the Fermi energy level ($E_F = 0$) within an energy range of -0.48 to 0.25 eV having a transmission coefficient up to 1.65 for Z_P, which gets reduced on adsorption. Although the overall transmission pattern between the energy range of -1 to 1 eV stay similar, but the value of transmission coefficient is drastically reduced in adsorbed configuration. It can arise due to the interaction between the atomic energy levels of adenine molecule and C_3N monolayer. A similar reduction in the transmission coefficient was also found for other DNA/RNA molecules adsorbed on the ZNR i.e about 40%, 39.6%, 37.5%,

View Article Online
DOI: 10.1039/D0CP00546K

Published on 08 April 2020. Downloaded by Université de Paris on 4/11/2020 4:02:23 PM.

Physical Chemistry Chemical Physics Accepted Manuscript

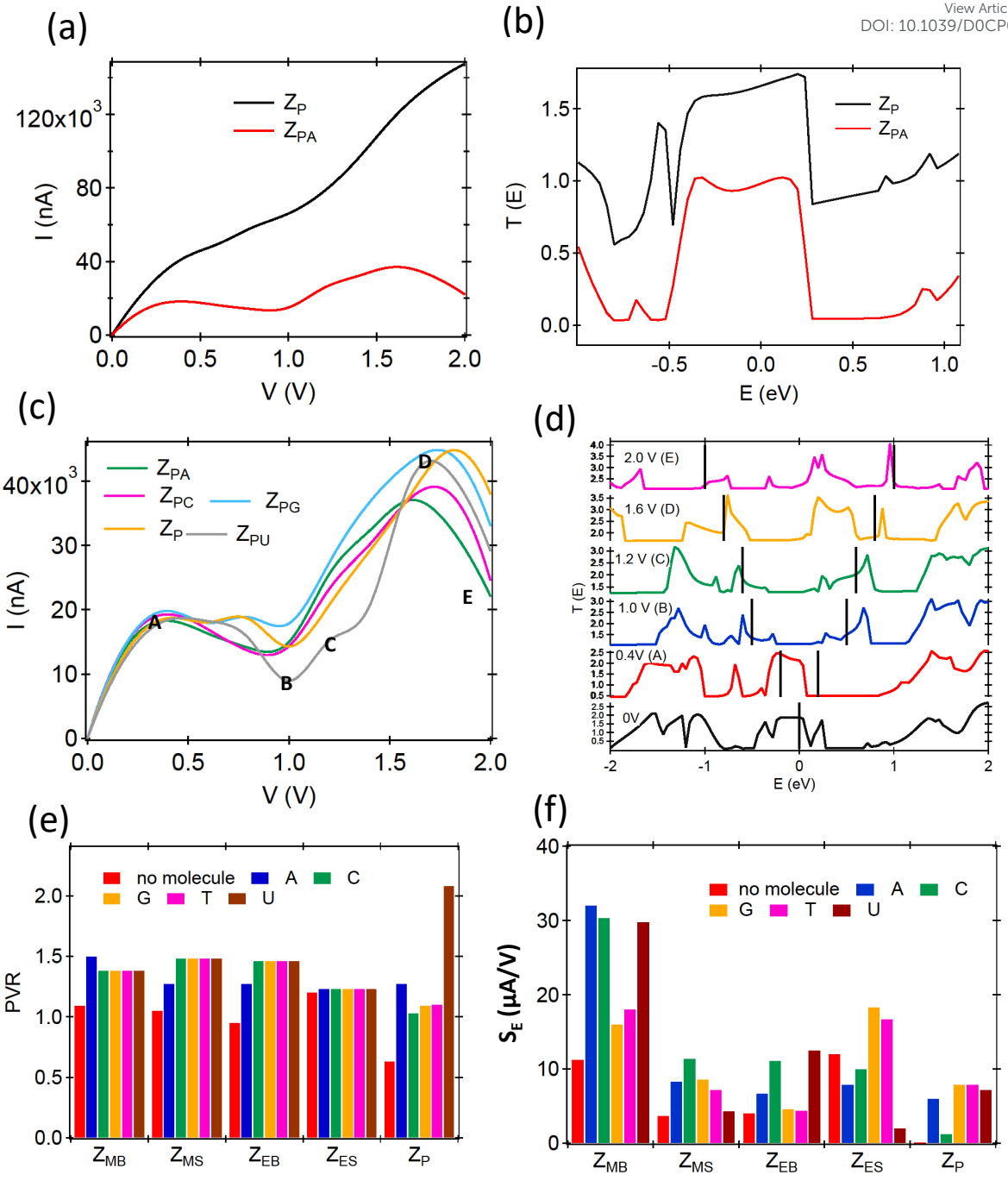

FIG. 2: (a) The current voltage characteristics and (b) Transmission coefficient of C_3N monolayer in pristine and adenine adsorbed configuration at a bias $\sim$ 0.1 V. (c) I-V characteristics of C_3N adsorbed with various DNA/RNA molecules. (d) The transmission spectrum corresponding to the different points A, B, C, D, E in Fig. 2c for Z_{PU}. (e) The peak to valley ratio and (f) switching efficiency of C_3N nanoribbon in pristine and various adsorbed configurations.

View Article Online
DOI: 10.1039/D0CP00546K

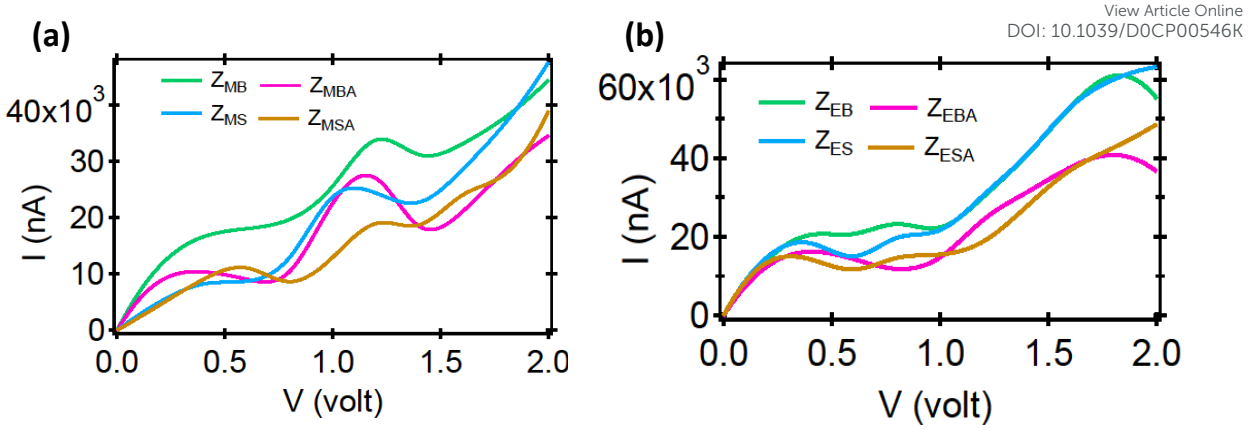

FIG. 3: The IV-characteristics of boron and sulphur doped ZNR at (a) middle and (b) edge location in the pristine and adsorbed configuration.

42.8% and 43.8% for Z_{PA}, Z_{PC}, Z_{PG}, Z_{PT} and Z_{PU} respectively near the Fermi level as estimated from the transmission spectrum given in Fig.S2 [41]. The inter-atomic interaction between C_3N and DNA molecules are the prime suspects behind this reduction in the value of transmission coefficient. In the presence of Adenine, the maximum reduction in current is observed to be $\sim 125\mu$A, around 85% lower than the current measured in the pristine configuration. Such a huge change of conductivity response in the presence of an adsorbed molecule suggests that the ZNR is sensitive to the presence of a nucleobase, which can be used for sensing such molecules.

The current-voltage characteristics of C_3N and various DNA/RNA molecules attached on the C_3N monolayer are shown in Fig. 2c. A general trend of oscillatory behaviour of current can be observed with increasing bias voltage in these adsorbed configurations. In the case of Z_{PU}, this behaviour constitutes of a linear increase in current between $0 \rightarrow 0.4$ V, (b) followed by decreasing between $0.4\text{V} \rightarrow 1\text{V}$, (c) again increasing from $1\text{V} \rightarrow 1.75$ V and (d) decreasing thereafter. The reduction in current with an increase in voltage is a signature of negative differential resistance effect (NDR) which has direct applications in oscillator, frequency modulators etc. and is observed in the C_3N system for the first time. This NDR response can be explained from the evolution of the transmission spectrum at different bias voltages (respective points marked as A, B, C, D, E), which represent the sum of the probability of all the electrons moving in a two probe system as illustrated in Fig.2d. At zero bias, the transmission window is absent, which at 0.4 V reaches a maximum of 2.46. Compared to this, the T(E) value is reduced at 0.8V, despite having a larger bias window

Published on 08 April 2020. Downloaded by Université de Paris on 4/11/2020 4:02:23 PM.

Physical Chemistry Chemical Physics Accepted Manuscript

View Article Online
DOI: 10.1039/D0CP00546K

for integration. The current increases after 1.2V as the value of transmission is increased along with a larger bias window for integration and the value of current is reduced at 2V to 29.1μA, which can be clearly observed from the reduction in the transmission as shown in Fig.2d.

To further quantify the NDR effect in ZNR under different conditions, we have used two different parameters [42] which are relevant for evaluating the performance of device operation. These are defined as,

$$\mathrm{PVR} = \frac{\mathrm{I_{peak}}}{\mathrm{I_{valley}}} \tag{2}$$

$$\mathrm{S_E} = \frac{\mathrm{I_{peak}} - \mathrm{I_{valley}}}{\mathrm{V_{peak}} - \mathrm{V_{valley}}} \tag{3}$$

PVR stands for peak to valley ratio and S_E indicates switching efficiency, where I_{peak}, I_{valley} and V_{peak}, V_{valley} are the current and voltage in peak (point A in Fig.2c) and valley (point B in Fig.2c) position in the I-V curve.

The distribution of the PVR and S_E for various cases has been shown in Fig.2e and Fig.2f respectively. It is to be noted that no NDR was not observed in the pristine configuration and it was only observed upon introduction of dopant atom and attachment of DNA/RNA molecules to the ZNR. The PVR of the Z_{PU} system is found to be 2.08 which is almost double in magnitude than the other adsorbed configuration like Z_{PA}, Z_{PG}, Z_{PT} (with comparable values). The switching efficiency on the other hand is of equal magnitude for Z_{PG}, Z_{PT}, Z_{PU}, while the lowest is observed for Z_{PC} with a value of 1.2 μA/V. Combining the PVR and S_E, Uracil attachment seems to offer maximum sensitivity towards the NDR response compared to other molecules. The observation of NDR on adsorption of a foreign molecule indicates the tunability obtained in electronic behaviour of a ZNR in the presence of a DNA/RNA molecule.

B. Effect of Doping

To understand the effect of doping, we have considered both p/n-type dopants, namely boron and sulphur at two different locations middle/edge. It was performed by selectively placing the dopant atom at the desired site as shown in Fig. S3(a-d) [41]. Here, we have also examined the effect of doping on ZNR with various attached DNA objects. The total

Published on 08 April 2020. Downloaded by Université de Paris on 4/11/2020 4:02:23 PM.

Physical Chemistry Chemical Physics Accepted Manuscript

View Article Online
DOI: 10.1039/D0CP00546K

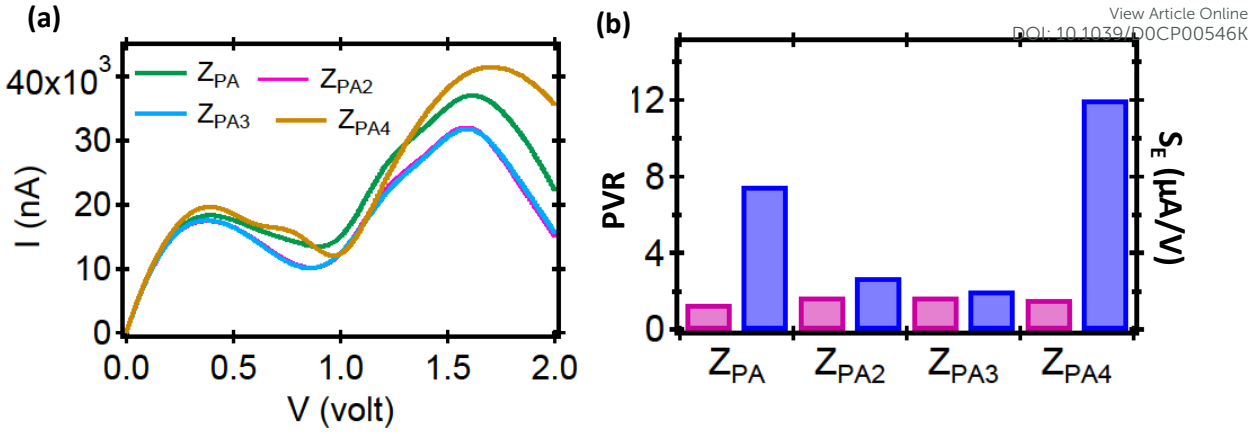

FIG. 4: (a) IV-characteristics and (b) PVR and Switching efficiency of C_3N nanoribbon for different concentration of adsorbed adenine molecules.

energy gets reduced on sulphur doping and increase on boron doping at both edge and middle locations. However, it does not change much with a change in the doping locations on the ZNR as shown in Fig.1b. The total energy gets further reduced after adsorption of the DNA molecules.

The current-voltage characteristics of ZNR doped with sulphur/boron atoms at middle/edge locations is shown in Fig. S4 [41]. Clear signature of current oscillations is observed indicating the presence of NDR in the doped system independent of the doping type/location. In addition to this, there is a reduction in current in the presence of the dopant atoms in the ZNR. It was observed that in the doped system, the amount of current flow is relatively higher for edge doping compared to the middle doping between a bias range of 1.2→2.0V. In the presence of Adenine, the I-V characteristics in various doped configurations is shown in Fig. 3(a-b). The amount of current flow is decreased in doped C_3N as a result of adsorption as explained in respective cases at 1.2 V; (i) 33.7 μA for Z_{MB}, (ii) 24.2 μA for Z_{MS} (iii) 30.7 μA for Z_{EB}, (iv) 30.7 μA for Z_{ES}. However, the oscillatory behaviour of the IV-pattern giving rise to the NDR features earlier, is also present in the Adenine adsorbed configurations and for other DNA/RNA molecules as well. The reduction in current flow is also common for other DNA/RNA molecules for both dopant types and locations. The transmission spectrum in various cases have been shown in Fig. S11 in the SI [41].

The PVR and S_E estimated for all the molecules in the doped configuration is given in Fig. 2(e-f). For adenine, maximum PVR of 1.5 and S_E equal 32 μA/V was found for

Published on 08 April 2020. Downloaded by Université de Paris on 4/11/2020 4:02:23 PM.

Physical Chemistry Chemical Physics Accepted Manuscript

View Article Online
DOI: 10.1039/D0CP00546K

Published on 08 April 2020. Downloaded by Université de Paris on 4/11/2020 4:02:23 PM.

Z_{MBA} and the PVR stays between 1.23-1.27 for other doped configurations, while the value of S_E is reduced drastically between the range of 6-32 μA/V. The PVR for C, G, T and U adsorbed cases are estimated at (i) 1.38 for Z_{MB}, (ii) 1.48 for Z_{MS}, (iii) 1.46 for Z_{EB} and (iv) 1.23 for Z_{ES}. Except adenine and uracil, these values are higher than PVR values calculated in respective unadsorbed configuration. A varied distribution of S_E was observed for various doping configuration in the presence of DNA/RNA molecules. The maximum S_E for A, C and U molecules were found for Z_{MB} configuration with values of (i) 32 μA/V, (ii) 30.3 μA/V (C) and (iii) 29.8 μA/V (U). For C and U these values are significantly higher compared to other configuration as illustrated in Fig. 2f. Comparable values of S_E were estimated for G and T adsorbed configurations (Z_{MB} and Z_{ES}) with values of 16 μA/V (Z_{MBG}), 18.3 μA/V (Z_{ESG}), 18 μA/V (Z_{MBT}) and 16.7 μA/V (Z_{EST}). These values are higher than the values estimated for unadsorbed cases. The overall pattern of S_E suggests that Z_{MB} offers a maximum in S_E for the adsorbed molecules. The PVR on the other hand does not show any such marked contrast between different doping geometries. Overall, the changes in S_E are significantly large as a result of doping and adsorption. Combining the PVR and S_E response, it can be concluded that Z_{MB} is preferred for adenine, cytosine, uracil while both Z_{ES} and Z_{MB} offer equally good performances for guanine and thymine adsorbed cases in terms of NDR performances. It suggests that the NDR related performances in C_3N nanoribbon can be improved through charge doping and adsorption of DNA/RNA molecules, offering additional tunability for related applications.

C. Effect of concentration

The effect of concentration of DNA/RNA molecules on the transport behaviour of ZNR is illustrated in Fig. 4(a-b). The concentration of adenine molecule attached to ZNR was varied from one molecule to four molecules, attaching them to the single/both edges as given in Fig. S5 [41]. These configuration are named as Z_{PA} (one adenine molecule attached to Z_P) and Z_{PA2}, Z_{PA3}, Z_{PA4} for similar configurations with 2, 3, 4 adenine molecules respectively. With an increase in the number of attached molecules the total energy becomes more negative. The reduction in energy is 24.18% (for Z_{PA}), increasing to 93.8% (Z_{PA4}) compared to Z_P. The adsorption energy (E_a) of 1, 2, 3, 4 numbers of adenine molecules was found to be 1.13 eV, 1.91 eV, 2.46 eV and 2.75 eV on Z_P respectively, which suggests an enhancement

Physical Chemistry Chemical Physics Accepted Manuscript

View Article Online
DOI: 10.1039/D0CP00546K

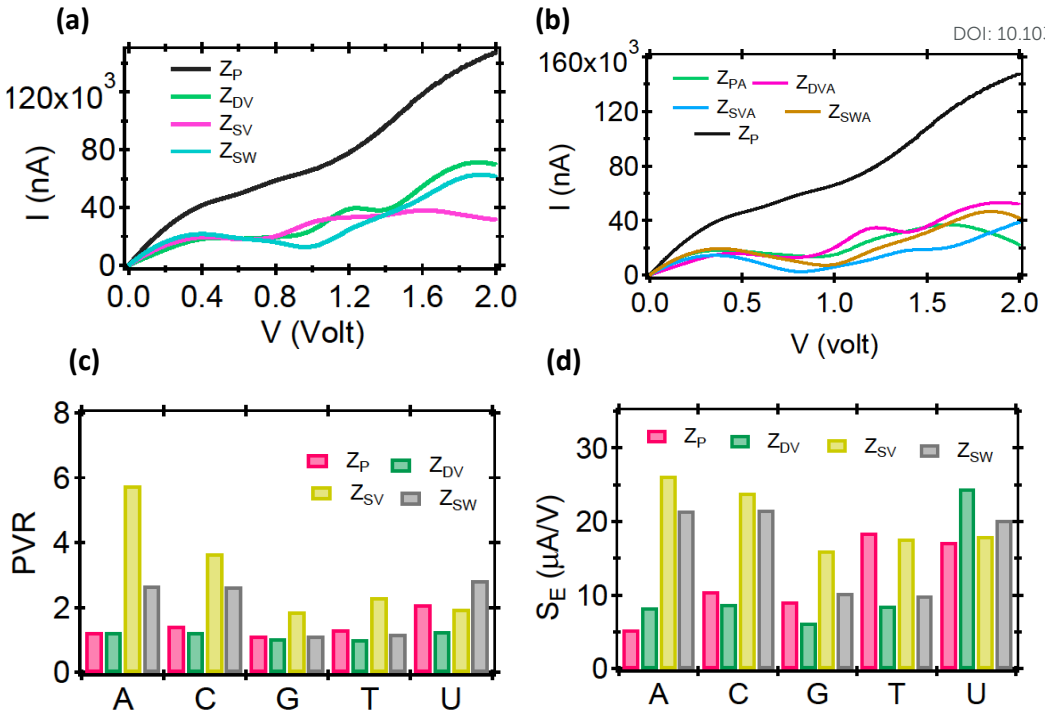

FIG. 5: The IV-characteristics of C_3N ZNR in various defect configurations in (a) unadsorbed and (b) adenine molecule adsorbed scenario. (c) The peak to valley ratio and (d) switching efficiency of C_3N nanoribbon in various defect geometries.

in the interaction between the layer and molecule with the increase in concentration of the molecule.

The current voltage characteristics of above mentioned system is given in Fig. 4a. At low applied bias, the I-V profile is similar for all the four cases which shows measurable dispersion. At higher applied bias between 1.2 - 2 V, the maximum current was measured for Z_{PA4} and minimum for Z_{PA2} and Z_{PA3}, with a maximum difference of 20.5 μA at 2 V, the periodic modulations of the I-V pattern indicates the presence of NDR in all the attached configurations. The maximum PVR of 1.7 was estimated for Z_{PA2} and Z_{PA3}, while the maximum of S_E equals 12 μA/V for Z_{PA4}. In terms of NDR response, Z_{PA4} offers the best combination of PVR and S_E among all the configurations. However, the effect of molecular attachment was preferential to a specific side. In the present analysis, current enhancement is higher when the adenine molecule is attached at the bottom part of the nanoribbon.

Published on 08 April 2020. Downloaded by Université de Paris on 4/11/2020 4:02:23 PM.

Physical Chemistry Chemical Physics Accepted Manuscript

View Article Online
DOI: 10.1039/D0CP00546K

Published on 08 April 2020. Downloaded by Université de Paris on 4/11/2020 4:02:23 PM.

Physical Chemistry Chemical Physics Accepted Manuscript

D. Effects of Defects

In order to study the effect of defects on the properties of C_3N nanoribbon, three separate defect configurations were investigated in the present work. These are namely; (i) single vacancy (SV), (ii) double vacancy (DV) and (iii) stone wales (SW) as shown in Fig. S6 (a-c) [41]. Single vacancy defect (Z_{SV}) refers to a position in which a single atom is absent from the normal lattice site in nanoribbon. In case of Double vacancy defect (Z_{DV}), two neighbouring atoms are removed from their regular lattice site and for stone wales defect (Z_{SW}) two neighbouring atoms undergo a 90° twist. The total energy of the ZNR in various defect configurations in the unadsorbed/adsorbed cases is shown in Fig. S6(d).

The I-V characteristics of various defect configurations are shown in Fig.5a. it was observed that there is reduction in current as defect is introduced in C_3N nanoribbon. The oscillating behaviour of current-voltage characteristics indicated the NDR behaviour which was further quantified from the PVR and S_E behaviour as shown in Fig 5(c-d). In Fig. 5a, major dispersions in I-V pattern was observed at higher applied voltages between 0.75 - 2V. For example, at 1.85V, 70.5μA current flow across Z_{DV} which is 8.6μA and 35.9 μA higher than Z_{SW} and Z_{SV} respectively. The transmission spectrum in respective cases is shown in Fig. S12 in the SI [41]. In the adenine molecule adsorbed configuration in Fig.5b the I-V patterns are well dispersed over the entire bias range 0.85-2V. Overall the current is higher for Z_{DVA} compared to Z_{SWA} followed by Z_{SVA}. This suggests that the I-V response can be tuned with specific type of vacancy in ZNR. At 2.0 V the current in all the defect adsorbed configurations (Z_{SVA}, Z_{DVA}, Z_{SWA}) are higher than Z_{PA} with a maximum difference of 29.9 μA. The NDR feature is also prevalent for Z_{SV}, Z_{DVA}, Z_{SWA}. Similar modulation in I-V pattern was also observed for various DNA/RNA molecules attached in the presence of various defect configurations. In Fig. 5c, the PVR is highest for Z_{SVA} followed by Z_{SVC}, Z_{SWU} and Z_{SWA}. Among various defect configurations; SV for adenine (A), cytosine (C), guanine (G), thymine (T) and SW for uracil (U) offer maximum PVR. The S_E in Fig. 5d also follows a similar trend, with highest S_E for adenine, cytosine, guanine and thymine in SV configuration and DV for uracil. It can be clearly seen that the PVR and S_E values are enhanced in the presence of defects in the nanoribbon in various adsorbed configurations. Considering the changes in the I-V pattern, PVR and S_E response, it can be clearly mentioned that defect is an effective way to tune the transport behaviour of the ZNR which can

View Article Online
DOI: 10.1039/D0CP00546K

be very useful for detecting the presence of a specific nucleobase. In the presence of vacancy or dopant atoms in the nanoribbon, the transmission pathways change significantly from the pristine case, which is an usual suspect behind the observed changes in current.

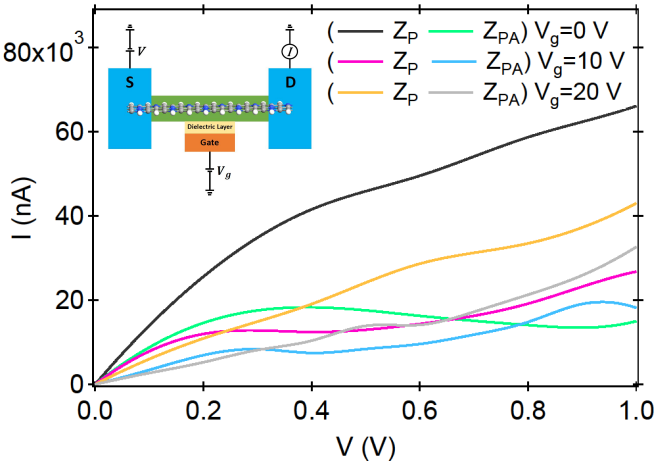

FIG. 6: IV-characteristcs of C_3N ZNR in the presence of a gate voltage in a FET geometry, (inset) Schematic representation of the FET structure.

E. Effect of Gate on C_3N

In the presence of a gate electrode, the carrier density can be controlled locally in a nanoribbon which is commonly used in a FET structure. In the present study, we have designed FET structure to understand the effect of gate electrode on transport properties of zigzag C_3N nanoribbon as shown in the inset of Fig. 6. The central region of C_3N monolayer is connected with a metallic gate electrode through dielectric layer of dielectric constant $\sim 10\epsilon_0$. The source and drain electrodes are made of ZNR. It offers the advantage of absence of potential barriers arising from metal-semiconductor contacts and its effect on transport properties. The I-V pattern for various gate voltages in the pristine and adsorbed configurations is shown in Fig.6. In the pristine case, significant changes in the current is observed with a maximum enhancement $\sim$ 15 μA (94.26%) from V_g = 10 V to 20 V. In the adenine adsorbed case, the difference stays of similar magnitude ($\sim$ 14.24μA). However, the value of current is reduced for Z_P from V_g = 0 to V_g = 10V, which is clear from the transmission spectrum given in Fig. S10 in the SI [41]. The maximum reduction in current at V_g = 20 V is 14.9 μA (at 0.633V) corresponding to a nearly 100% change. Similarly at V_g = 10V, a change in current of 8.48 μA was observed at 2V applied bias. These results suggest

Published on 08 April 2020. Downloaded by Université de Paris on 4/11/2020 4:02:23 PM.

Physical Chemistry Chemical Physics Accepted Manuscript

View Article Online
DOI: 10.1039/D0CP00546K

that applications of a gate voltage is an effective way to control the transport behaviour of a C_3N nanoribbon, which in the presence of an adsorbed molecule shows distinct changes as desired for sensing application. This can be very useful for the control and tuning of the performance of a C_3N based biosensor, without making any permanent damage to the structure [43, 44].

F. Experimental feasibility and detection sensitivity

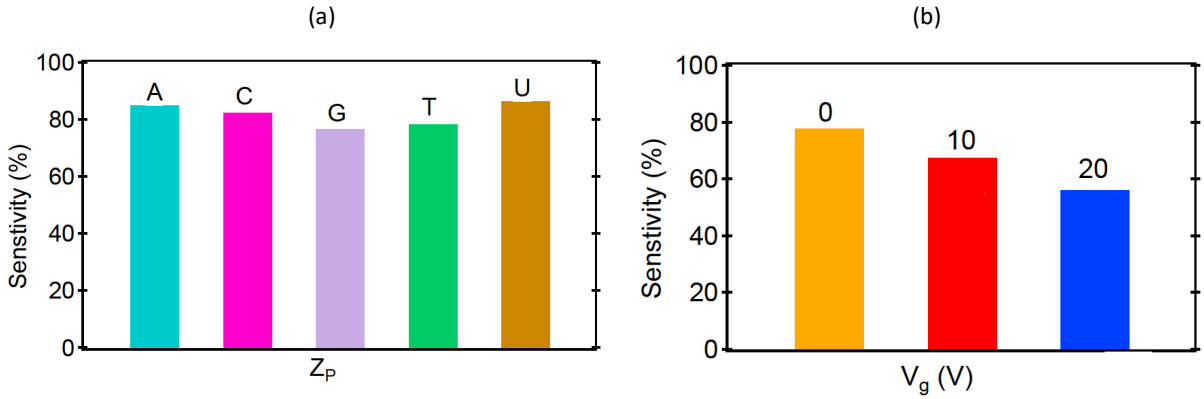

FIG. 7: Variation in the Sensitivity of C_3N nanoribbon (a) in the presence of DNA/RNA nucleobases and (b) at different gate voltage towards adenine (A) molecule.

DNA sequencing is experimentally performed using various solid state nanopores made with: (i) protein like alpha hemolysin/MspA porin [45–48], (ii) silicon/glass membrane [7] or (iii) 2D-material like Graphene/MoS_2 [49]. Typical dimension of the nanopore lies between 2 - 25 nm diameter, which can be produced using ion-beam sculpting, electron beam lithography etc. During the sequencing process, DNA-bases are passed through the nanopore with a very high speed (in the order of 1 - 10 nucleobase per microsecond) in the presence of an applied bias of 10 - 100 mV and the resulting ionic current is measured $\sim$ nA. The thermodynamic response of the sequencing process can be simulated using MD (Molecular dynamics) which also predicted a current of similar order of magnitude in a time scale $\sim$ 300 ps.

The sensitivity of detection of a specific nucleobase can be defined as,

$$S = \frac{(I_p - I_{ad})}{I_p} \times 100\% \tag{4}$$

Published on 08 April 2020. Downloaded by Université de Paris on 4/11/2020 4:02:23 PM.

Physical Chemistry Chemical Physics Accepted Manuscript

View Article Online
DOI: 10.1039/D0CP00546K

Published on 08 April 2020. Downloaded by Université de Paris on 4/11/2020 4:02:23 PM.

Where I_{ad} and I_p are the values of current(s) in the presence and absence of nucleobase, respectively. The sensitivity (S) of various nucleobases on pristine C_3N is illustrated in Fig. 7a. The maximum S was estimated for U (86.4%) with minimum of (76.5%) for G. The sensitivity was found to increase moderately with an increase in the concentration of the nucleobase, which for adenine (A) molecule varied between a range of 84.8% - 88.96% as given in Fig. S8a in the SI [41]. In the presence of defect in nanoribbon, it reaches to highest value of 95.61% for Adenine in the presence of single vacancy. In the presence of a gate voltage, the highest sensitivity is observed at $V_g = 0$V with a value of 77.65% for Adenine, which however reduces with an increase in the V_g. Details of sensitivity estimated for C_3N under different circumstances can be found in Fig. S7 and Fig. S8 in the SI [41]. Earlier studies suggests that the sensitivity is significantly higher than graphene and of similar order of magnitude with MoS_2 based systems [50, 51]. However, the current estimated in our case $\sim$ 100 μA range, which is significantly higher than these systems and also offer a large change in current on adsorption of the DNA molecule. In the sub-10 nm structure as used in the present investigation, C_3N offers a range of superior attributes which makes it a potential candidate for DNA/RNA detection and biosensing applications.

V. CONCLUSIONS

In this work, we have investigated the transport properties of a newly discovered 2D material, C_3N through first-principles based NEGF-DFT methodology in the proximity of various DNA and RNA nucleobases. The energy calculation revealed that the system becomes more stable in the adsorbed configuration, while the current-voltage response demonstrates distinct changes between the pristine and adsorbed configurations. For Adenine, it offers a maximum change in current of 125 μA (85%), suggesting its usefulness as a sensor of such molecules. Further tunability of the transport response can be obtained in the presence of doping and defects. Extensive studies revealed that edge doping is more effective than centre doping, offering a higher level of conduction, while significant changes in the current is observed for various defect geometries as well, with a maximum in the presence of DV in the ZNR. Increase in the concentration of attached molecules resulted in an increase in the conduction, however, specific to the adsorbed geometries. In the presence of a gate voltage, an almost 100% change in the current is observed between the pristine and adsorbed config-

Physical Chemistry Chemical Physics Accepted Manuscript

View Article Online
DOI: 10.1039/D0CP00546K

uration, offering an effective way to control the sensing response in a non-invasive manner. The observation of NDR has been reported for the first time in the C_3N ZNR system, which was quantified via the estimation of PVR and S_E with value > 30 μA/V. Our current observations demonstrates the usefulness of C_3N nanoribbon for the sensing of various DNA/RNA nucleobases and various biological objects. It also offers an effective route to design next generation sequencing architectures, label free biosensor of superior sensitivity and energy efficient nanoscale designs etc.

VI. CONFLICT OF INTEREST

There are no conflicts to declare.

VII. ACKNOWLEDGEMENT

SR thanks the CSIR for financial support. SJR acknowledges the financial support received through DST-INSPIRE Grant (Ref: DST/INSPIRE/04/2015/003087), DST-ECR Grant (Ref. ECR/2017/002223) and DST-CRG (Ref. CRG/2019/003289).

Published on 08 April 2020. Downloaded by Université de Paris on 4/11/2020 4:02:23 PM.

Physical Chemistry Chemical Physics Accepted Manuscript

View Article Online
DOI: 10.1039/D0CP00546K

Published on 08 April 2020. Downloaded by Université de Paris on 4/11/2020 4:02:23 PM.

[1] F. Sanger, S. Nicklen, and A. R. Coulson, Proceedings of the National Academy of Sciences 74, 5463 (1977).

[2] C. Dekker, Nat. Nanotechnol 2, 209 (2007).

[3] D. Branton, D. W. Deamer, A. Marziali, H. Bayley, S. A. Benner, T. Butler, M. Di Ventra, S. Garaj, A. Hibbs, X. Huang, et al., Nature Biotechnology 26, 1146 EP (2008).

[4] Asma Wasfia, Falah Awwada, Ahmad I.Ayeshb, Biosensors and Bioelectronics, 119, 191-203 (2018).

[5] Stephanie J. Heerema, Cees Dekker, Nature Nanotechnology, 11, 127136 (2016).

[6] Zuzanna S. Siwy, Matthew Davenport, Nature Nanotechnology volume 5, 697698 (2010).

[7] S. Garaj, W. Hubbard, A. Reina, J. Kong, D. Branton, and J. A. Golovchenko, Nature 467, 190 (2010).

[8] A. J. Storm, J. H. Chen, H. W. Zandbergen, and C. Dekker, Phys. Rev. E 71, 051903 (2005).

[9] A. B. Farimani, K. Min, and N. R. Aluru, ACS Nano 8, 7914 (2014).

[10] S. Rani and S. Ray, Carbon 144, 235 (2019)

[11] A. K. Geim and K. S. Novoselov, Nature Materials 6, 183 (2007).

[12] K Kumari, A Kumar, DK Kotnees, J Balakrishnan, AD Thakur, SJ Ray, Journal of Alloys and Compounds 815, 152213 (2020)

[13] JF Dayen, SJ Ray, O Karis, IJ Vera-Marun, MV Kamalakar, Applied Physics Reviews 7 (1), 011303 (2020)

[14] S. J. Ray and L. Alff, physica status solidi (b) 254, 1600163 (2017).

[15] J. Mahmood, E. K. Lee, M. Jung, D. Shin, H.-J. Choi, J.-M. Seo, S.-M. Jung, D. Kim, F. Li, M. S. Lah, et al., Proceedings of the National Academy of Sciences 113, 7414 (2016).

[16] S. Yang, W. Li, C. Ye, G. Wang, H. Tian, C. Zhu, P. He, G. Ding, X. Xie, Y. Liu, et al., Advanced Materials 29, 1605625 (2017).

[17] M. Makaremi, B. Mortazavi, and C. V. Singh, The Journal of Physical Chemistry C 121, 18575 (2017).

[18] M. Makaremi, S. Grixti, K. T. Butler, G. A. Ozin, and C. V. Singh, ACS Applied Materials & Interfaces 10, 11143 (2018).

[19] X. Zhou, W. Feng, S. Guan, B. Fu, W. Su, and Y. Yao, Journal of Materials Research 32,

Physical Chemistry Chemical Physics Accepted Manuscript

View Article Online
DOI: 10.1039/D0CP00546K

2993?3001 (2017).

[20] H. Zeng, J. Zhao, A.-Q. Cheng, L. Zhang, Z. He, and R.-S. Chen, Nanotechnology 29, 075201 (2018).

[21] A. Chaudhury, S. Majumder, and S. J. Ray, Phys. Rev. Applied 11, 024056 (2019).

[22] Y. Hong, J. Zhang, and X. C. Zeng, Nanoscale 10, 4301 (2018).

[23] S. Kumar, S. Sharma, V. Babar, and U. Schwingenschlogl, J. Mater. Chem. A 5, 20407 (2017).

[24] X. Li, L. Zhu, Q. Xue, X. Chang, C. Ling, and W. Xing, ACS Applied Materials & Interfaces 9, 31161 (2017).

[25] D. Ma, J. Zhang, X. Li, C. He, Z. Lu, Z. Lu, Z. Yang, and Y. Wang, Sensors and Actuators B: Chemical 266, 664 (2018), ISSN 0925-4005.

[26] X. Li, T. Guo, L. Zhu, C. Ling, Q. Xue, and W. Xing, Chemical Engineering Journal 338, 92 (2018), ISSN 1385-8947.

[27] P. Bhauriyal, A. Mahata, and B. Pathak, The Journal of Physical Chemistry C 122, 2481 (2018).

[28] Yanan Zhou, Guoping Gao, Jun Kang, Wei Chu, and Lin-Wang Wang, J. Mater. Chem. A, 7, 12050-12059 (2019).

[29] S. J. Ray, Sensors and Actuators B: Chemical 222, 492 (2016).

[30] S. J. Ray, M. V. Kamalakar, and R. Chowdhury, Journal of Physics: Condensed Matter 28, 195302 (2016).

[31] Heping Cui, Kai Zheng, Yingying Zhang, Huaiyu Ye, Xianping Chen, IEEE ELECTRON DEVICE LETTERS, 39, 2, (2018).

[32] Zijia Zhao, Yongliang Yong, Song Hu, Caitao Li, and Yanmin Kuang, AIP Advances 9, 125308 (2019).

[33] Fatih Ersan, Ethem Aktrk, Salim Ciracib, Carbon, 143, 329-334 (2019).

[34] F. Ersan, O. zengi Aktrk, E. Aktrk, S. Ciraci, J. Phys. Chem. C, 122, 26, 14598-14605 (2018).

[35] M. Brandbyge, J.-L. Mozos, P. Ordej?on, J. Taylor, and K. Stokbro, Phys. Rev. B 65, 165401 (2002).

[36] Atomistix toolkit, Quantum Wise Division.

[37] J. P. Perdew, K. Burke, and M. Ernzerhof, Phys. Rev. Lett. 77, 3865 (1996).

[38] H. J. Monkhorst and J. D. Pack, Phys. Rev. B 13, 5188 (1976), URL https://link.aps.org/doi/10.1103/PhysRevB.13.5188.

Published on 08 April 2020. Downloaded by Université de Paris on 4/11/2020 4:02:23 PM.

Physical Chemistry Chemical Physics Accepted Manuscript

View Article Online
DOI: 10.1039/D0CP00546K

[39] R. Landauer, IBM Journal of Research and Development 32, 306 (1988), ISSN 0018-8646.

[40] M. Buttiker, Y. Imry, R. Landauer, and S. Pinhas, Phys. Rev. B 31, 6207 (1985),

[41] S. Rani *et al.*, See supporting information for additional results on *Two-dimensional C_3N based sub-10 nanometer Biosensor.*

[42] S. J. Ray and M. V. Kamalakar, Phys. Chem. Chem. Phys. 20, 13508 (2018).

[43] A. K. Nair, P. Kumari, M. Venkata Kamalakar and S. J. Ray, Phys. Chem. Chem. Phys., 21, 23713 (2019).

[44] P. Kumari, S. Majumder, S. Rani, A. K. Nair, K. Kumari, M. Venkata Kamalakar and S. J. Ray, Physical Chemistry Chemical Physics, 22, 5893 - 5901 (2020)

[45] Stefan Howorka, Stephen Cheley and Hagan Bayley, Nature biotechnology, 19, 636 (2001).

[46] J. Cao, E. Ertekin, V. Srinivasan, W. Fan, S. Huang, H. Zheng, J. W. L. Yim, D. R. Khanal, D. F. Ogletree, J. C. Grossman and J. Wu, Nature Nanotechnology, 4, 266, (2009).

[47] David Stoddart, Andrew J. Heron, Ellina Mikhailova, Giovanni Maglia, and Hagan Bayley, Proc. Natl Acad. Sci. USA 106, 7702-7707 (2009).

[48] Ian M. Derrington, Tom Z. Butler, Marcus D. Collins, Elizabeth Manrao, Mikhail Pavlenok, Michael Niederweis, and Jens H. Gundlach, Proc. Natl Acad. Sci. USA 107, 16060-16065 (2010).

[49] Christopher A. Merchant, Ken Healy, Meni Wanunu, Vishva RayNeil Peterman, John Bartel, Michael D. Fischbein, Kimberly Venta, Zhengtang Luo, A. T. Charlie Johnson, Marija Drndi, Nano Lett., 10, 2915-2921 (2010).

[50] Zongyou Yin, Qiyuan He, Xiao Huang, Juan Zhang, Shixin Wu, Peng Chen, Gang Lu, Peng Chen, Qichun Zhang, Qingyu Yana and Hua Zhang, Nanoscale, 4, 293 (2012).

[51] Deblina Sarkar, Wei Liu, Xuejun Xie, Aaron C. Anselmo, Samir Mitragotri, Kaustav Banerjee, ACS Nano, 8 3992-4003 (2014).

Published on 08 April 2020. Downloaded by Université de Paris on 4/11/2020 4:02:23 PM.

Physical Chemistry Chemical Physics Accepted Manuscript